Observation of phonon structure in electron density of states of a normal metal

A. Knigavko[1], J. P. Carbotte[1] and F. Marsiglio[2]

[1] *Department of Physics and Astronomy, McMaster University, Hamilton, Ontario, Canada, L8S 4M1*

[2] *Department of Physics, University of Alberta, Edmonton, Alberta, Canada, T6J 2J1*

PACS. 71.10.Ay – Fermi-liquid theory and other phenomenological models.
PACS. 71.38.-k – Polarons and electron-phonon interactions.
PACS. 79.60.-i – Photoemission and photoelectron spectra.

Abstract. – Within standard treatments of the interacting electron–phonon system the electron density of states (EDOS) shows no sign of the phonons when the system is in the normal state. On the other hand, emergence of a fine energy scale in the superconducting state makes the phonons readily observable in the EDOS and other spectroscopic quantities. Here we wish to re-examine the conditions under which phonon structure might be present in the normal state. Accounting for a finite, i.e. non-infinite, electronic bandwidth results in easily distinguishable phonon structure in the EDOS. We argue that for narrow band metals, the resolution of photoemission spectroscopy is sufficient for resolving these structures. Manifestations of finite band effects in K_3C_{60} are discussed.

Introduction. – The observation of phonon structure in tunneling data for superconducting materials became a very important diagnostic tool in the 1960's [1]. Following this initial success attempts were made (with some degree of success) to extract similar information in the normal state [2–4]. Part of the difficulty at the time no doubt was due to the fact that calculations using many-body Green functions predicted that no phonon structure should be present in the Electronic Density Of States (EDOS) [5, 6]. When the bare EDOS is infinitely wide and featureless and when particle-hole symmetry is present, the dressed EDOS retains its constant bare band value and the phonon signatures drop out. On the other hand, as was studied extensively in the 1980's (see for instance [7, 8]), phonon renormalizations do enter when the EDOS has significant energy dependence near the Fermi surface on the scale of phonon energies.

More recently [9–14] it was realized that phonon structure can also arise when a finite band cutoff is applied in the EDOS on the scale of the bandwidth. In this letter we want to accomplish two goals: first we want to understand under what conditions these structures can be resolved in Angle Integrated Photo Emission Spectroscopy (AIPES) and/or tunneling even for relatively broad bands, and secondly, we wish to establish the scale of the structures for parameters more specific to a real narrow band material, in this case K_3C_{60}. While our primary interest here is in the EDOS we also provide comparison with other spectroscopic

quantities such as the real and imaginary parts of the quasiparticle self energy and its optical counterpart, the memory function, both of which have phonon signatures even when the band is assumed to be infinite. It is well known that even when these structures are not directly visible, as in the optical scattering rate, they can be emphasized either by differentiation [15], or extracted by other more sophisticated "inversion" procedures [15, 16]. In contrast, the phonon structures due to a finite bandwidth are more readily detectable.

To see sizeable features in the EDOS, the electron-phonon interaction must be sufficiently strong. To be specific we consider the Eliashberg $\alpha^2F(\omega)$ function appropriate to the intermediate coupling strength superconductor K_3C_{60}. We start with a large bare bandwidth $W = 2.5$ eV and find that for the clean system and at low temperature the phonon structure in the renormalized EDOS is very prominent in the range of phonon energies (keep in mind that for an infinite bandwidth the structure is absent). Furthermore, the presence of impurity scattering does not obliterate the structure; it merely reduces its size [12]. Reducing the bare bandwidth to $W = 0.5$ eV, a value more relevant for K_3C_{60}, we find that all dominant features of the renormalized EDOS are determined by the electron–phonon interaction.

Bare EDOS, the self energy and the renormalized EDOS. – We use the following model for the bare electronic band: $N_0(\xi) = N_0\Theta\left(W/2 - |\xi|\right)$, where W is the bare band width and $\Theta(x)$ is the step function. The constant N_0 is fixed by normalization: $N_0 = 1/W$. In this letter we retain particle-hole symmetry for simplicity, with the chemical potential at the center of the band, $\mu = 0$.

The electronic self energy $\Sigma(z) = \Sigma_1(z) + \mathrm{i}\Sigma_2(z)$ is calculated from the Migdal equations formulated in the mixed real–imaginary axis representation [12, 17]:

$$\begin{aligned}
\Sigma(z) &= \Gamma\,\eta(z) + T\sum_{m=-\infty}^{+\infty}\lambda(z-\mathrm{i}\omega_m)\eta(\mathrm{i}\omega_m) \\
&+ \int_0^\infty \mathrm{d}\omega\,\alpha^2F(\omega)\left\{\left[f(\omega-z)+n(\omega)\right]\eta(z-\omega) + \left[f(\omega+z)+n(\omega)\right]\eta(z+\omega)\right\}, \quad (1)\\
\lambda(z) &= \int_0^\infty \mathrm{d}\omega\,\alpha^2F(\omega)\frac{2\omega}{\omega^2-z^2}, \quad (2)\\
\eta(z) &= \int_{-\infty}^\infty \mathrm{d}\xi\,\frac{N_0(\xi)}{N_0(0)}\frac{1}{z-\xi-\Sigma(z)}, \quad (3)
\end{aligned}$$

where $\omega_m = \pi T(2m-1)$, $m \in Z$ are the fermionic Matsubara frequencies, and $f(\omega)$ and $n(\omega)$ are the Fermi and Bose distribution functions respectively. The electron–phonon interaction is specified in terms of the electron–phonon spectral function $\alpha^2F(\omega)$ (the Eliashberg function). The parameter Γ, which has the meaning of an impurity scattering rate, specifies the strength of the interaction with impurities. Note that finding $\Sigma(z)$ requires a self consistent solution of eqs. (1)–(3), which is a consequence of accounting for the finite bare band width in eq. (3).

The variable z can assume arbitrary complex values. At first, the solutions for $\Sigma(z)$ are sought on the imaginary axis, at $z = \mathrm{i}\omega_m$, where eq. (1) is simpler. Then, the function $\eta(\mathrm{i}\omega_m)$ is used to set up an iterative procedure to find $\Sigma(\omega)$ just above the real axis (we use ω as shorthand for $\omega + \mathrm{i}0^+$). While we will focus on the EDOS, which can be determined in AIPES experiments, the real axis self energy, both its real and imaginary parts, can be obtained from the angular-resolved photoemission. The accuracy of this technique has increased dramatically in recent years and properties of both new and traditional materials have been scrutinized (see, for example, refs. [18–21] for a flavour of the recent developments).

Motivated by the electron–phonon interaction in the fulleride compound K_3C_{60}, we use a

three frequency model for the electron-phonon spectral function:

$$\alpha^2F(\omega) = \lambda \sum_{i=1}^{3} \frac{\omega_i l_i}{2} \delta(\omega - \omega_i), \qquad \sum_{i=1}^{3} l_i = 1 \tag{4}$$

with $l_1 = 0.3, l_2 = 0.2, l_3 = 0.5$ and $\omega_1 : \omega_2 : \omega_3 = 0.04 : 0.09 : 0.19$ eV [22]. The interaction strength a is defined as the area under the $\alpha^2F(\omega)$ curve. The mass enhancement parameter λ is given by eq. (2) with $z = 0$. For the forthcoming discussion we set $\lambda = 0.71$. Then this model has $a = 43.8$ meV and $\omega_{\ln} = 102.5$ meV, where $\omega_{\ln}$ is the logarithmic frequency [6], a convenient parameter to quantify the phonon energy scale. In the last section we consider different values of λ as well. Finally, below we use $W = 2.5$ eV.

The renormalized density of electronic states (or density of states for quasiparticles) is defined by

$$N(\omega) = \int_{-\infty}^{+\infty} \mathrm{d}\xi N_0(\xi) A(\xi, \omega), \tag{5}$$

where $A(\xi, \omega) = -\operatorname{Im} G_{ret}(\xi, \omega)/\pi$ is the electronic spectral density and $G_{ret}(\xi, \omega)$ is the retarded Green function. It can be expressed in terms of the function $\eta = \eta_1 + \mathrm{i}\eta_2$ of Eq. (3) through $N(\omega)/N_0(0) = -\eta_2(\omega)/\pi$. In AIPES the measured intensity, $I(\omega)$, is the product of the renormalized EDOS and a thermal factor $f(\omega)$ which provides a cutoff at $T = 0$, convoluted with the instrument resolution $R(\omega)$ which can be taken as a Gaussian with half-width of 2.8 meV [20]. With particle–hole symmetry it is convenient to define a symmetrized quantity $I_s(\omega) = [I(\omega) + I(-\omega)]/2$ from which $f(\omega)$ drops out [23], leading to

$$I_s(\omega) = \int_{-\infty}^{\infty} \mathrm{d}\omega' N(\omega') R(\omega' - \omega). \tag{6}$$

In fig. 1 we show results (solid curves) for I_s vs ω and compare with the density of states $N(\omega)$ (dotted curves). The main frame is for $T \simeq 72.5K$ while the inset is for $T = 14.5$ K. Two different scattering rates are used, namely the clean case $\Gamma = 0$ (top curves) and $\Gamma = a/2 \approx 22$ meV (bottom curves). For the clean case the curves start at value unity at zero frequency. The introduction of impurity scattering reduces the value of the density of states in the low frequency range shown in fig. 1 but does not significantly smear the predicted phonon structure. Three drops are clearly seen at the frequencies of each of the three delta functions in the model spectral density $\alpha^2F(\omega)$ of eq. (4). We note that increasing the impurity scattering does not smear out the predicted phonon structure, rather it reduces the effective step drop. On the other hand, comparison of the inset with the main frame shows that temperature does smooth out the curves considerably, but even for the worst case $T = 72.5$ K and $\Gamma = 22$ meV, the structure in $I_s(\omega)$ remains. For the chosen parameters, which are not extreme, instrument resolution does not have a strong smearing effect. We also used a representative extended $\alpha^2F(\omega)$ with the same λ and position of the peaks as in eq. (4). In this case the results (dashed curve) for $N(\omega)$ and $I_s(\omega)$ are indistinguishable on the scale of fig. 1.

Another way to detect the finite band phonon structures in the EDOS is through tunneling spectroscopy. The well known formula for the current, I (assuming the tunneling matrix element is independent of energy), through a tunnel junction reads:

$$I(V) \sim \int_{-\infty}^{+\infty} \mathrm{d}\xi \frac{N_L(\xi)}{N_L(0)} \frac{N_R(\xi)}{N_R(0)} \left[f(\xi) - f(\xi + eV) \right], \tag{7}$$

where V is the applied voltage, e is the charge of the electron and the labels L and R denote materials on opposite sides of the junction. The normalization of $N_{L,R}(\omega)$ is to its value at

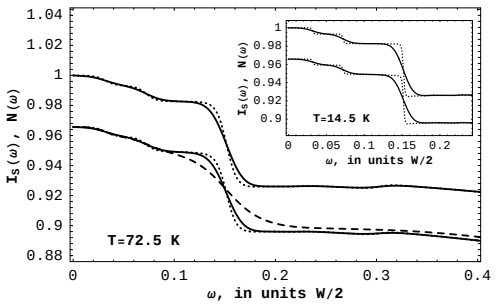

Fig. 1

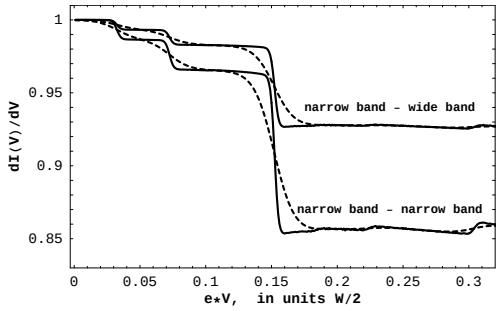

Fig. 2

Fig. 1 – Comparison of the renormalized density of states $N(\omega)$ (dotted) with the symmetrized photoemission signal $I_s(\omega)$ (solid) that includes the instrument resolution for $\alpha^2F(\omega)$ of eq. (4). The impurity scattering rate is $\Gamma = 0$ and 22 meV for the upper and lower pairs of curves respectively. Frequency ω is given in units of half bare bandwidth $W/2 = 1.25$ eV. The temperature is $T = 72.5$ K. For a representative extended $\alpha^2F(\omega)$ the results (dashed curve) for $N(\omega)$ and $I_s(\omega)$ are indistinguishable on the scale of the plot. Inset: the same as the main frame but for $T = 14.5$ K.

Fig. 2 – Differential I–V chacteristic for tunelling between two identical narrow band (i.e. W = 2.5 eV) metals (lower two curves) and between narrow and wide band metals (upper two curves). The temperature is $T = 14.5$ K (solid curves) and 72.5 K (dashed curves), and the impurity scattering rate is $\Gamma = 22$ meV.

$\omega = 0$. In fig. 2 we show $\mathrm{d}I(V)/\mathrm{d}V$ vs $e * V$ for a narrow band – wide band case (upper pair of curves) and for the case where the same narrow band metal is on both sides (lower pair of curves). The impurity scattering rate is $\Gamma = a/2 \approx 22$ meV and the two temperatures shown are $T = 14.5$ K and 72.5 K. In both cases the phonon structures are clearly identifiable in the differential conductance even at higher temperatures. The upper curves are almost identical to normalized EDOS $N(\omega)/N(0)$ (see inset in fig. 1). Features in the lower curves are about twice as large in magnitude as in the upper curves. Finite band effects are enhanced when the same narrow band metal is used on each side of tunnel junction.

Optical response. – For characterization of the optical response the quantity of interest is the memory function. Its real and imaginary parts are $\tau_{op}^{-1}(\omega)$ and $-\omega\lambda_{op}(\omega)$ respectively, where τ_{op}^{-1} is the optical scattering rate and λ_{op} is the optical mass renormalization [6]. The memory function is connected to the optical conductivity $\sigma = \sigma_1 + \mathrm{i}\sigma_2$ by algebraic relations: $\tau_{op}^{-1} = (2S/\pi)\Re[1/\sigma]$ and $-\omega\lambda_{op} = \omega - (2S/\pi)\Im[1/\sigma]$, where S is the total optical spectral weight defined as $S = \int_0^{+\infty} \mathrm{d}\omega\sigma_1(\omega)$. The optical conductivity for our model was obtained using linear response theory, neglecting vertex corrections. The result for the real part reads:

$$\sigma_1(\omega) \;=\; \frac{2\pi e^2}{\hbar^2}\int_{-\infty}^{+\infty}\mathrm{d}\xi N_0(\xi)v_\xi^2\int_{-\infty}^{\infty}\mathrm{d}\omega' A\left(\xi,\omega'\right)A\left(\xi,\omega'+\omega\right)\frac{f\left(\omega'\right)-f(\omega'+\omega)}{\omega}, \quad (8)$$

where v_ξ^2 is the averaged square of the group velocity (see Ref. [24] for details). We assume that the system is isotropic and use for v_ξ^2 the expression $v_\xi^2 = \frac{2\hbar^2}{mD}\left(\frac{W}{2}+\xi\right)$, derived from the quadratic dispersion of free electrons with lower band edge at $\xi = -W/2$. Here D is the number of spatial dimensions, m the free electron mass. Since the complex conductivity $\sigma(\omega)$ satisfies the Kramers–Kronig relation, the required imaginary part can be obtained as the Hilbert transform of the real part.

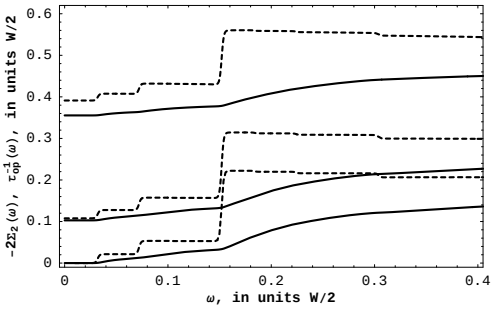

Fig. 3

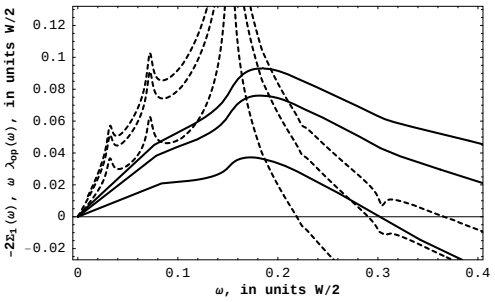

Fig. 4

Fig. 3 – Comparison of the quasiparticle scattering rate $-2\Sigma_2(\omega)$ (dashed) with its optical counterpart τ_{op}^{-1} (ω) (solid) for impurity scattering rates $\Gamma = 0$, 22, and 88 meV, from bottom to top. The temperature is $T = 14.5$ K, the bare bandwidth is $W = 2.5$ eV.

Fig. 4 – Comparison of $-2\Sigma_1(\omega)$ (dashed) with $\omega\lambda_{op}(\omega)$ (solid) for the same values of Γ as in fig. 3, but now from top to bottom. The temperature is $T = 14.5$ K, the bare bandwidth is $W = 2.5$ eV.

The memory function is the optical counterpart of the self energy. In fig. 3 we compare $\tau_{op}^{-1}(\omega)$ with $-2\Sigma_2(\omega)$ in the limited range of frequencies $\omega \in [0, 500]$ meV for $T = 14.5$ K. In the infinite band case these quantities are equal at $\omega = 0$. The bottom pair of curves in fig. 3 is for the clean case, the middle pair is for $\Gamma = a/2 \approx 22$ meV, while the top pair is for $\Gamma = 2a \approx 88$ meV. The effect of increasing the impurity content is to push the curves up corresponding to a larger value of the residual scattering. Beyond this effect there are changes in phonon structures, but little smearing. The structures are much more visible in the quasiparticle scattering rate $-2\Sigma_2$ (steps) than in the corresponding optical quantity τ_{op}^{-1}, which has only small kinks at frequencies related to the three oscillators of the model $\alpha^2F(\omega)$ given by Eq. (4). Of course, it is well known that optical data is encoded with the information on the phonons even in the infinite band case. However, a second derivative of the data is required [15], and this is normally not as accurate.

In fig. 4 we plot $\omega\lambda_{op}(\omega)$ (solid curves) and $-2\Sigma_1(\omega)$ (dashed curves) for the same values of Γ as those for fig. 3. In this case both quantities become smaller as impurity scattering increases in the frequency range shown. Note that all curves cross zero, which is a characteristic of finite bands. The crossing frequency depends on Γ for both $\omega\lambda_{op}(\omega)$ and $-2\Sigma_1(\omega)$, with the former dependence stronger. Note that in fig. 4 the phonon structures are again much more prominent in the self energy as compared with its optical counterpart.

Very narrow bands. – So far we have considered the case of a rather wide though finite electronic band with full width $W = 2.5$ eV where $W \gg \omega_{\ln}$ and the phonon structures in EDOS have a generic form. However, band structure calculations for one family of the known narrow materials — fulleride compounds — give a much smaller value $W = 0.5$ eV [25, 26]. One expects that in this situation many of the discussed features should be significantly enhanced [13]. In fig. 5 we present the renormalized EDOS $N(\omega)$ as a function of frequency ω at $T = 14.5$ K for the model $\alpha^2F(\omega)$ of eq. (4) relevant to K_3C_{60}. The bare EDOS was approximated by a flat EDOS with width 0.5 eV, and with $\mu = 0$ (dot–dashed curve). The results shown are for impurity scattering rates $\Gamma = 4.4$ and 39.9 meV, as indicated. We used two values of the mass enhancement parameter: $\lambda = 0.71$ [10], which is representative of the range quoted in the literature [22, 27], and a bigger value $\lambda = 2.0$, which may be in a range more realistic for the fullerides [28].

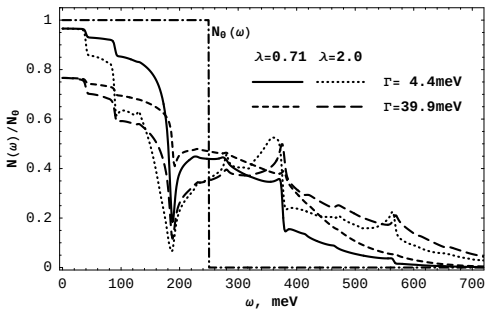

Fig. 5

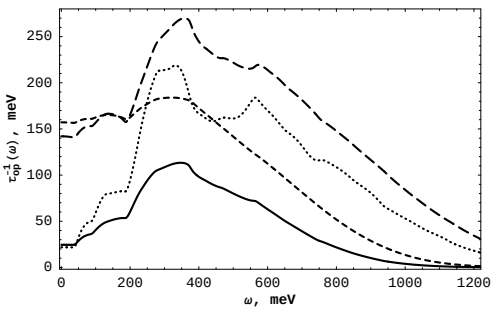

Fig. 6

Fig. 5 – The renormalized density of states $N(\omega)/N_0$ as a function of frequency ω for the model $\alpha^2F(\omega)$ of eq. (4) relevant to K_3C_{60}. The curves differ by values of λ and Γ as indicated. The dot–dashed curve is the bare EDOS with $W = 0.5$ eV. The temperature is $T = 14.5$ K.

Fig. 6 – The optical scattering rate $\tau_{op}^{-1}(\omega)$ as a function of frequency ω for the K_3C_{60} model of eq. (4). Parameters and marking of the curves are the same as in fig. 5.

In fig. 5 we see that inclusion of the electron–phonon interaction modifies the entire band, even for the modest value of $\lambda = 0.71$. The renormalized EDOS extends well beyond $\omega = W/2 = 250$ meV. Note that what determines the energy of the highest steep drop in $N(\omega)$ is not the bare band edge but rather the energy of the third phonon mode $\omega_3 = 190$ meV, which has the strongest coupling to band electrons in the model of eq. (4). Beyond this energy the multiphonon structures appear, with magnitude depending both on λ and on Γ; this extends the renormalized band beyond $2.5 \times (W/2)$. On the other hand, no prominent feature corresponding to the bare band edge remains in the renormalized EDOS.

The sharp drop in renormalized EDOS in fig. 5 at $\omega \approx \omega_3$ is in good quantitative agreement with photoemission data on both polycrystalline [27] and monolayer samples [29,30] of metallic fullerides. We note that the model of $\alpha^2F(\omega)$ defined in eq. (4) is expected to work reasonably well even for two dimensional samples of fullerides because the stronger coupled ω_3 mode is associated mainly with intramolecular vibrations of C_{60} [31]. The flat bare EDOS is also appropriate for the two dimensional electonic bands. We conclude that in a very narrow band metallic material the electron–phonon interactions have a very profound impact on the density of electronic states observable by various spectroscopies, to such an extent that they can dominate $N(\omega)$.

The importance of electron–phonon interactions and multiboson processes in understanding photoemission data in fullerides has been emphasized by Knupfer *et al.* [27]. Using a different approach they analysed the magnitude of $N(0)$ and redistibution of electronic states derived from the bare band over frequency. In this letter we pointed out the significance of finite band effects and provided a useful method to treat other aspects of the problem, such as the effect of impurities, within the same formalism. Sensitivity of these effects to the value of λ could possibly be used to extract the mass enhancement parameter for fulleride compounds from experimental data on the EDOS, supplemented by the other spectroscopic techniques. As an example, in fig. 6 we show results for the optical scattering rate in the K_3C_{60} of eq. (4) at $T = 14.5$ K. The curves shown are for $\lambda = 0.71$ and 2.0, and $\Gamma = 4.4$ meV and 39.9 meV. They are marked the same way as in fig. 5. Note that, similarly to the case of the EDOS, the phonon structures dominate the frequency behavior of $\tau_{op}^{-1}(\omega)$ for very narrow band metals.

* * *

Work is supported by the Natural Science and Engineering Research Council of Canada (NSERC) and the Canadian Institute for Advanced Research (CIAR).

REFERENCES

[1] W.L. McMillan and J.M. Rowell, in *Superconductivity*, edited by R.D. Parks (Marcel Dekker, Inc., New York, 1969), p. 561.
[2] F. Steinrisser, L.C. Davis and C.B. Duke, Phys. Rev. **176**, 912 (1968).
[3] T.T. Chen and J.G. Adler, Solid State Commun. **8**, 1965 (1970).
[4] See, for example, E.L. Wolf, *Principles of Electron Tunneling Spectroscopy*, (Oxford University Press, New York, 1985), for a thorough discussion.
[5] S. Englesberg and J.R. Schrieffer, Phys. Rev. **131**, 993 (1963).
[6] F. Marsiglio and J.P. Carbotte, in *The Physics of Superconductivity*, Vol. I: *Conventional and High T_c Superconductors*, edited by K.H. Bennemann and J.B. Ketterson (Springer Verlag, Berlin, 2003), p. 233.
[7] See, for example, a series of comprehensive articles by B. Mitrović and J.P. Carbotte, Can. Jour. Phys. **61**, 758 (1983); Can. Jour. Phys. **61**, 784 (1983); Can. Jour. Phys. **61**, 872 (1983).
[8] W.E. Pickett, Phys. Rev. B **26**, 1186 (1982).
[9] A.S. Alexandrov, V.N. Grebenev, and E.A. Mazur, Pis'ma Zh. Eksp. Teor. Fiz. **45** 357 (1987) [JETP Lett. **45** 455 (1987)].
[10] J.-W. Yoo and H.-Y. Choi, Phys. Rev. B **62**, 4440 (2000).
[11] E. Cappelluti, C. Grimaldi, and L. Pietronero, Phys. Rev. B **64**, 125104 (2001).
[12] E. Cappelluti and L. Pietronero, Phys. Rev. B **68**, 224511 (2003).
[13] F. Doğan and F. Marsiglio, Phys. Rev. B **68**, 165102, (2003).
[14] A. Knigavko and J.P. Carbotte, Phys. Rev. B **72**, 035125 (2005).
[15] F. Marsiglio, T. Startseva, and J.P. Carbotte, Phys. Lett. A **245**, 172 (1998).
[16] S.V. Dordevic, C.C. Homes, J.J. Tu, T. Valla, M. Strongin, P.D. Johnson, G.D. Gu, and D.N. Basov, Phys. Rev. B**71**, 104529 (2005)
[17] F. Marsiglio, M. Schossmann, and J.P. Carbotte, Phys. Rev. B **37**, 4965 (1988).
[18] T. Valla, A.V. Fedorov, P.D. Johnson, and S.L. Hulbert, Phys. Rev. Lett. **83**, 2085 (1999).
[19] A. Chainani, T. Yokoya, T. Kiss, and S. Shin, Phys. Rev. Lett. **85**, 1966 (2000).
[20] F. Reinert, B. Eltner, G. Nicolay, D. Ehm, S. Schmidt, and S. Hufner, Phys. Rev. Lett. **91**, 186406 (2003).
[21] T.P. Devereaux, T. Cuk, Z.-X. Shen, and N. Nagaosa, Phys. Rev. Lett. **93**, 117004 (2004).
[22] H.-Y. Choi, Phys. Rev. Lett. **81**, 441 (1998).
[23] M.R. Norman, H. Ding, M. Randeria, J.C. Campuzano, T. Yokoya, T. Takeuchi, T. Takahashi, T. Mochiku, K. Kadowaki, P. Guptasarma, and D.G. Hinks, Nature, **382**, 157 (1998).
[24] F. Marsiglio and J.E. Hirsch, Physica C **165**, 71 (1990).
[25] S. Satpathy, V.P. Antropov, O.K. Andersen, O. Jepsen, O. Gunnarsson, and A.I. Liechtenstein, Phys. Rev. B **46**, 1773 (1992).
[26] M.P. Gelfand, Supercond. Review **1**, 103 (1994).
[27] M. Knupfer, M. Merkel, M.S. Golden, J. Fink, O. Gunnarsson, and V.P. Antropov, Phys. Rev. B **47**, R13944 (1993).
[28] For $W \approx \omega_{\ln}$ the value of λ extracted from electronic self energy using the infinite band relation $\lambda = -\mathrm{d}\Sigma_1(\omega = 0)/\mathrm{d}\omega$ can be noticably smaller than the one calculated from $\alpha^2 F(\omega)$ [12].
[29] W.L. Yang, V. Brouet, X.J. Zhou, S.G. Louie, M.L. Cohen, S.A. Kellar, P.V. Bogdanov, A. Lanzara, A. Goldoni, F. Parmigiani, Z. Hussain, and Z.-X. Shen, Science **300**, 303 (2003).
[30] W.L. Yang, V. Brouet, X.J. Zhou, Z. Hussain, and Z.-X. Shen, unpublished [2005 APS March meeting, report Y13.00006].
[31] O. Gunnarsson, Rev. Mod. Phys. **69**, 575 (1997).